GEOPHYSICS

10.1126/sciadv.1600427

Stability of Fe,Al-bearing bridgmanite in the lower mantle and synthesis of pure Fe-bridgmanite

Leyla Ismailova,[1,2]* Elena Bykova,[1] Maxim Bykov,[1] Valerio Cerantola,[1,3] Catherine McCammon,[1] Tiziana Boffa Ballaran,[1] Andrei Bobrov,[4] Ryosuke Sinmyo,[1] Natalia Dubrovinskaia,[2] Konstantin Glazyrin,[5] Hanns-Peter Liermann,[5] Ilya Kupenko,[1,3,6] Michael Hanfland,[3] Clemens Prescher,[7] Vitali Prakapenka,[7] Volodymyr Svitlyk,[3] Leonid Dubrovinsky[1]*

The physical and chemical properties of Earth's mantle, as well as its dynamics and evolution, heavily depend on the phase composition of the region. On the basis of experiments in laser-heated diamond anvil cells, we demonstrate that Fe,Al-bearing bridgmanite (magnesium silicate perovskite) is stable to pressures over 120 GPa and temperatures above 3000 K. Ferric iron stabilizes Fe-rich bridgmanite such that we were able to synthesize pure iron bridgmanite at pressures between ~45 and 110 GPa. The compressibility of ferric iron–bearing bridgmanite is significantly different from any known bridgmanite, which has direct implications for the interpretation of seismic tomography data.

INTRODUCTION

The lower mantle constitutes more than half of Earth's interior by volume and is believed to consist predominantly of bridgmanite [perovskite-structured $(Mg,Fe)(Si,Al)O_3$] with up to approximately 20% ferropericlase (Mg,Fe)O by volume (*1*, *2*). Thus, the physical properties, crystal chemistry, and stability of bridgmanite at high pressures and temperatures are critical for understanding the structure and dynamics of our planet, as well as the interior of other terrestrial planets and exoplanets. Ever since the application of laser-heated diamond anvil cell (DAC) techniques and x-ray diffraction allowed the major components of the lower mantle to be identified (*3*), investigations of perovskite-structured silicates have been a popular focus of mineral physics studies. Over the decades, there have been several claims that bridgmanite undergoes structural transformations (*4*–*6*) or that the phase is not chemically stable at all conditions within the lower mantle (*7*–*9*). However, so far, only one phase transition in $(Mg,Fe)(Si,Al)O_3$ bridgmanite has been unambiguously confirmed, namely, to a $CaIrO_3$-type structure phase (often called post-perovskite) above ~125 GPa and at high temperatures (*6*). Earlier observations (*4*, *5*) of decomposition were probably due to large temperature gradients, resulting in Soret or Gorsky effects arising from one-sided highly focused laser heating (*9*, *10*). Recently, using more advanced setups for laser-heated DAC experiments, Zhang *et al.* (*8*) reported that Fe-bearing bridgmanite is unstable at pressures of 95 to 101 GPa and temperatures of 2200 to 2400 K, where it loses its iron component and decomposes into a nearly Fe-free $MgSiO_3$ perovskite and a Fe-rich $(Mg,Fe)SiO_3$ phase ("H-phase") with a hexagonal structure not previously known, causing a small volume reduction in bridgmanite. The hexagonal phase can be synthesized at pressures as low as ~85 GPa. These findings may be of primary relevance for geophysical, geochemical, and geodynamic models of the lower mantle below depths of 2000 km. Changes in the pseudobinary $MgSiO_3$-$FeSiO_3$ phase relations could be associated with spin crossover of iron above ~60 GPa and drastic modifications of its crystal chemistry. However, structural data on $(Mg,Fe)(Si,Al)O_3$ bridgmanite in the megabar pressure range and ~2000 K are very limited, and its possible decomposition with formation of the H-phase is inconsistent with some experimental observations and theoretical calculations (*5*, *11*–*14*). Here, we apply single-crystal x-ray diffraction (SCXRD) in laser-heated DACs (see Materials and Methods and the Supplementary Materials) to study stability of iron (and aluminum)–bearing bridgmanite at conditions of the deep part of Earth's lower mantle.

RESULTS

Single crystals of bridgmanite with different compositions, $Mg_{0.83}Fe_{0.17}Al_{0.06}Si_{0.94}O_3$ (referred to below as FE17), $Mg_{0.86}Fe_{0.14}Al_{0.04}Si_{0.96}O_3$ (FE14), and $Mg_{0.60}Fe_{0.40}Si_{0.63}Al_{0.37}O_3$ (FE40), as determined from SCXRD structural refinement and microprobe analysis, were selected from samples synthesized in a multianvil (MA) apparatus at 25 GPa and 1300°C. According to Mössbauer spectroscopy, the ratio $Fe^{3+}/\Sigma Fe$ is 0.93(3) (*12*) in FE40 and 0.20(3) in FE17 and FE14 (*15*). Before being loaded into a DAC, crystals with sizes from ~$10 \times 10 \times 5\ \mu m^3$ to ~$20 \times 20 \times 7\ \mu m^3$ were selected and tested with an in-house high-brilliance rotating anode diffractometer (*16*). X-ray diffraction measurements were carried out in angle-dispersive mode at the 13-IDD beamline ($\lambda = 0.31$ Å; beam size, $5 \times 5\ \mu m^2$) at the Advanced Photon Source (APS), United States, at the ID09a ($\lambda = 0.41$ Å; beam size, $10 \times 10\ \mu m^2$) and ID27 ($\lambda = 0.37$ Å; beam size, $3 \times 3\ \mu m^2$) beamlines at the European Synchrotron Radiation Facility (ESRF), France, and at the extreme conditions beamline P02.2 ($\lambda = 0.2903$Å; beam size, $3 \times 8\ \mu m^2$) The Positron-Electron Tandem Ring Accelerator III (PETRA III), Deutsches Elektronen-Synchrotron (DESY), Germany (see Materials and Methods for more details). The samples were loaded at ~1.4 kbar in Ne pressure-transmitting medium, compressed to pressures ranging from 32 to 130 GPa (Fig. 1), and heated

[1]Bayerisches Geoinstitut, University of Bayreuth, D-95440 Bayreuth, Germany. [2]Laboratory of Crystallography, University of Bayreuth, D-95440 Bayreuth, Germany. [3]European Synchrotron Radiation Facility, BP 220, Grenoble F-38043, France. [4]Department of Petrology, Geological Faculty, Moscow State University, 119234 Moscow, Russia. [5]Photon Science, Deutsches Elektronen-Synchrotron, Notkestrasse 85, D-22603 Hamburg, Germany. [6]Institut für Mineralogie, University of Münster, Corrensstrasse 24, 48149 Münster, Germany. [7]Center for Advanced Radiation Sources, University of Chicago, 9700 South Cass Avenue, Argonne, IL 60437, USA.
*Corresponding author. Email: leyla.isml@gmail.com (L.I.); leonid.dubrovinsky@uni-bayreuth.de (L.D.)

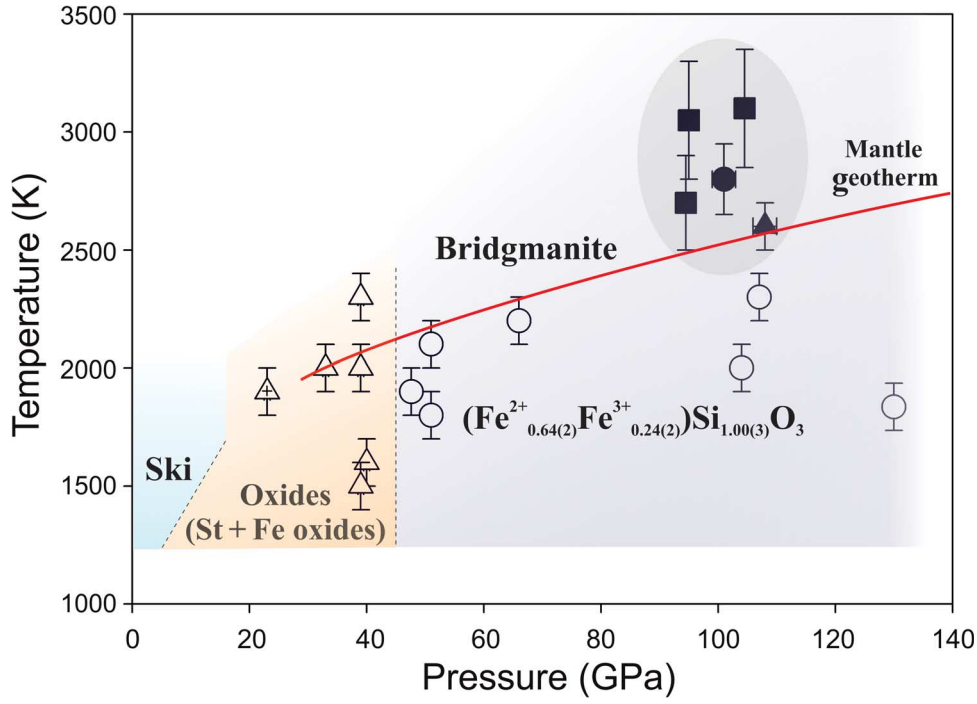

Fig. 1. Stability fields of skiagite garnet, oxides, and bridgmanite. Ski, skiagite-majorite garnet $Fe^{2+}_3(Fe^{2+}_{0.234(2)}Fe^{3+}_{1.532(1)}Si^{4+}_{0.234(2)})(SiO_4)_3$ (*25*); open triangle with cross, mixture of stishovite (St, SiO_2), $Fe_{1-x}O$, and Fe_4O_5; empty triangles, mixture of stishovite and Fe_4O_5. Solid symbols correspond to conditions of the experiments on $Mg_{0.86}Fe_{0.14}Al_{0.04}Si_{0.96}O_3$ (FE14, squares), $Mg_{0.83}Fe_{0.17}Al_{0.06}Si_{0.94}O_3$ (FE17, triangle), and $Mg_{0.60}Fe_{0.40}Si_{0.63}Al_{0.37}O_3$ (FE40, circle) described in table S1. Open circles show conditions at which pure iron bridgmanite ($Fe^{2+}_{0.64(2)}Fe^{3+}_{0.24(2)}Si_{1.00(3)}O_3$) was synthesized. The dark gray area marks pressure-temperature conditions at which experiments on Fe,Al-bearing bridgmanite were conducted. Red solid curve, expected lower mantle geotherm (*46*). Error bars indicate experimental uncertainty in pressure and temperature.

using a double-sided laser setup at temperatures between 2200 and 3100 K over relatively long time periods ranging from 20 to 100 min.

The only observed changes upon laser heating for all investigated samples were shifts in the positions of reflections due to variations in temperature and pressure (fig. S1). Detailed inspection of diffraction patterns (Fig. 2 and fig. S2) did not reveal the appearance of any non-identified reflections during or after heating. When pressure remained the same before and after laser heating (see, for example, table S1), the lattice parameters of bridgmanite also remained the same within experimental uncertainty, suggesting that the integrity of the material was not affected by prolonged laser heating. The data sets collected for temperature-quenched samples are of sufficient quality to perform accurate structure refinements, including the determination of the occupancy of iron at the two different distinct crystallographic sites of the perovskite-type structure [see the studies by Glazyrin *et al.* (*12*) and Bykova (*17*) for methodological details]. Perovskite-structured orthorhombic bridgmanite (space group *Pbmn*, no. 62) has two cation positions (fig. S3): one coordinated by a distorted bicaped prism ("A"-site) and one octahedrally coordinated ("B"-site). We found that in accordance with previous observations (*12*) and within the uncertainties of our method (about 5% of total iron content), there is no evidence for redistribution of Fe between the two crystallographic sites and there are no changes in the chemical composition (table S1).

The occurrence of an iron-rich H-phase at high pressures and temperatures may be related to the instability of pure iron bridgmanite [or pure ferrous iron bridgmanite (*8*)]. Indeed, the amount of the $Fe^{2+}SiO_3$ component that can be accommodated by Mg,Fe bridgmanite ranges from about 12 mole percent (mol %) at 26 GPa (*18*) to 50 to 74 mol % at ~85 GPa (*19*–*21*). At pressures from ~20 to over 115 GPa, pure $FeSiO_3$ was reported to disproportionate into FeO and SiO_2 (*22*, *23*). Ferrous iron end-member bridgmanite has never been synthesized so far, and the solubility limit of the Fe-bearing component in perovskite-structured silicate remains unknown. However, it is now widely accepted (*2*, *5*, *12*, *15*, *24*) that bridgmanite relevant to the lower mantle contains both ferrous and ferric iron. Thus, the relevant question is whether pure Fe^{2+},Fe^{3+}-bridgmanite exists or not.

We used synthetic skiagite-majorite garnet as the starting material for experiments to study the high-pressure high-temperature behavior of Mg,Al-free Fe^{3+}-bearing silicate with the composition $Fe^{2+}_3(Fe^{2+}_{0.234(2)}Fe^{3+}_{1.532(1)}Si^{4+}_{0.234(2)})(SiO_4)_3$, as determined from single-crystal diffraction and Mössbauer spectroscopy data (*25*). Our experiments using the MA apparatus up to 23 GPa and 1900 K demonstrate that above 12.5 GPa and 1700 K, skiagite-majorite garnet decomposes into SiO_2 and Fe oxides (Fig. 1 and fig. S4). Laser heating of skiagite-majorite garnet in the DAC up to ~40 GPa and 1500 to 2300 K resulted in decomposition into stishovite (SiO_2) and Fe_4O_5 (Fig. 1 and fig. S5) (*26*). Remarkably, in some runs, iron oxide crystallized in the form of single crystals (or polycrystalline domains), which gave diffraction data of sufficient quality for an accurate structure refinement of Fe_4O_5 (fig. S6 and table S4). Upon heating at pressures above ~45 GPa, we observed

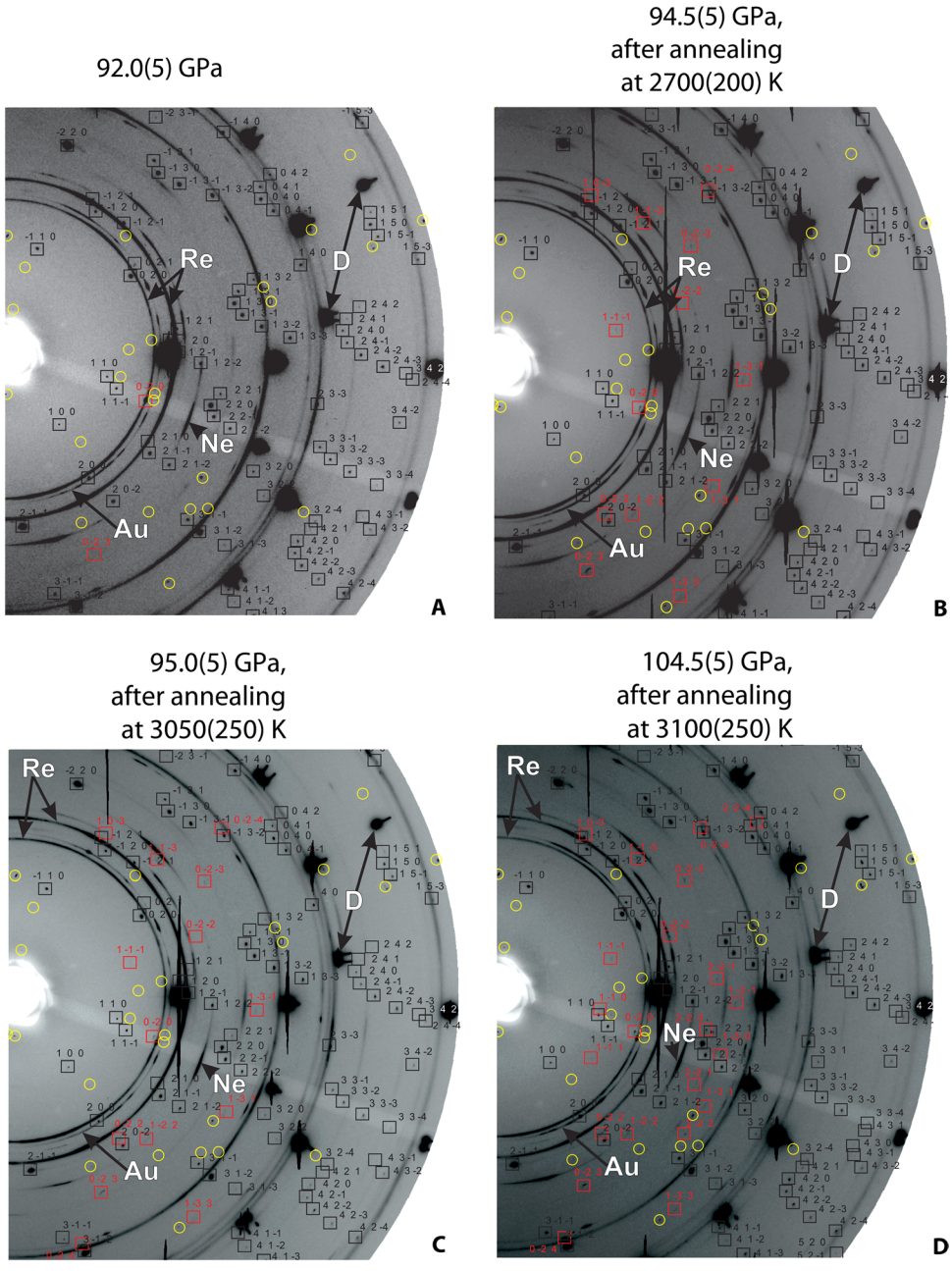

Fig. 2. Examples of parts of the two-dimensional wide-scan x-ray diffraction images of bridgmanite $Mg_{0.86}Fe_{0.14}Al_{0.04}Si_{0.96}O_3$. (**A** to **D**) Data were collected (A) before and (B to D) after laser heating at the indicated temperatures and pressures. Indices are given for bridgmanite reflections (underlined by boxes). The only observed changes in diffraction patterns upon heating are due to development of additional domains of the same phase (marked in red). Large black spots are due to diamond (D) reflections. Diffraction rings of Ne (pressure transmitting medium), Re (gasket), and Au are also marked. Data were collected at IDD-13 at APS. Yellow circles indicate bad pixels of the detector. (Full high-resolution images are also given in the Supplementary Materials).

different sequences of transformations. For example, at 51(1) GPa and 1800(100) K, skiagite-majorite garnet decomposes into stishovite, high-pressure orthorhombic h-Fe_3O_4 (*27*), and one additional phase (fig. S5). At higher temperatures [2100(100) K; for example, fig. S5], diffraction lines of stishovite are absent, the intensity of reflections of h-Fe_3O_4 decreases, and the diffraction pattern is dominated by lines of the additional phase that can be easily indexed as orthorhombic. Analysis of single-crystal diffraction data allows unambiguous identification of this phase to be $GdFeO_3$-type perovskite structure (fig. S3 and table S2). The same phase was synthesized by heating skiagite-majorite

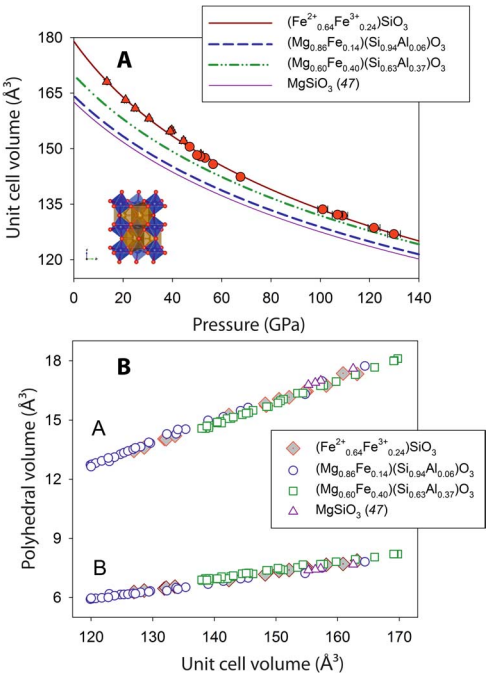

Fig. 3. Compressibility of $(Fe^{2+}_{0.64(2)}Fe^{3+}_{0.24(2)})Si_{1.00(3)}O_3$ silicate perovskite. (**A**) Unit cell volumes of single crystals of pure iron bridgmanite synthesized at different pressures were measured on compression (red dots with error bars) and decompression (red triangles with error bars). The data are fitted (solid dark red line) with a Birch-Murnaghan equation of state, giving bulk modulus of K_{300} = 190(4) GPa and unit cell volume at ambient conditions V_0 = 178.98(6) Å (K' = 4). For comparison, compressional curves of pure $MgSiO_3$ (solid purple line) (*32*, *47*), $(Mg_{0.6},Fe_{0.4})(Si_{0.63}Al_{0.37})SiO_3$ (dotted-dashed green line) (*12*, *34*), and $(Mg_{0.86},Fe_{0.14})(Si_{0.94}Al_{0.06})SiO_3$ (dashed dark-blue line) are shown (see also table S3). Insert shows model of perovskite-structured orthorhombic (space group *Pbmn*, no. 62) bridgmanite with two distinct cation coordinations: distorted bicaped prisms (A-site, brown) and octahedra (B-site, blue). (**B**) Dependence of A- and B-site polyhedral volumes as a function of unit cell volume for bridgmanite with different compositions (see text for more details and references).

garnet at different pressures up to over 100 GPa (Fig. 1 and table S2). Once synthesized, the phase maintains its structure on compression up to ~125 GPa and decompression down to at least 13 GPa. Accurate structure refinements of samples produced at different pressures and temperatures give highly consistent results regarding the composition of the material. On the basis of the results of six different experiments, it can be expressed as $(Fe^{2+}_{0.64(2)}Fe^{3+}_{0.24(2)})Si_{1.00(3)}O_3$ (Fig. 1 and table S2). Thus, we synthesized pure Fe-bridgmanite and demonstrated that above ~50 GPa, the presence of Fe^{3+} stabilizes bridgmanite relative to mixed oxides.

The crystal chemistry of ferric iron–bearing Fe-bridgmanite is remarkable (table S2). First, we observed that all iron is located in the A-site, and within the accuracy of determination of the occupancies of structural positions (better than 5%), there is no iron in the octahedra (B-site). This conclusion is robust because x-ray scattering factors of silicon and iron are very different, and agrees with recent studies on bridgmanite of different compositions (*10*, *12*, *15*). Second, it is obvious that the material synthesized between 50 and 100 GPa contains a significant amount of vacancies (about 12%) at the A-site according to the substitution scheme $3Fe^{2+} \rightarrow 2Fe^{3+}$ + vacancy. The formation of materials with vacancies at high pressure is not unprecedented, particularly among Fe^{3+}-bearing oxides (*28*), but has not been expected for bridgmanite (*29*, *30*). Nevertheless, on the basis of the summary of bridgmanite compositions known from the study by Liu *et al.* (*31*), it was reported that there are indications that an A-site vacancy is favored in Al-free bridgmanite, whereas an oxygen vacancy is dominant in Al-bearing bridgmanite.

The dependence of polyhedral volumes on the unit cell volume (Fig. 3) for Fe-bridgmanite is the same as for pure magnesium– and iron-aluminum–bearing bridgmanites. It confirms that the large iron cation does not enter the B-site because incorporation of any appreciable amount of iron cations in the octahedral site in Fe-bearing bridgmanite should significantly affect its compressibility.

The effect of pressure on the lattice parameters of Fe^{3+}-bearing Fe-bridgmanite is very different from the variation observed in any other silicate perovskites [see the studies by Dorfman *et al.* (*10*), Glazyrin *et al.* (*12*), Kupenko *et al.* (*24*), and Boffa Ballaran *et al.* (*32*) and references therein] in that the *a* and *b* axes are much more compressible (fig. S7). Thus, vacancies on the A-site lead to significant softening of the material; it has a bulk modulus of K_{300} = 190(4) GPa [K' = 4, V_0 = 178.98(6) $Å^3$ per unit cell; Fig. 3 and table S3], which is drastically lower than the values known for other Fe- or/and Al-rich bridgmanites (fig. S8) (*10*, *12*, *21*, *32*, *33*).

DISCUSSION

The elastic properties of Fe,Al-bearing bridgmanite reported in the literature are highly controversial, especially in cases where samples were synthesized in situ in laser-heated DACs [for discussion, see particularly the studies by Andrault (*5*), Dorfman *et al.* (*10*), Glazyrin *et al.* (*12*), Dorfman *et al.* (*21*), Boffa Ballaran *et al.* (*32*), and Saikia *et al.* (*33*)]. The large effect of Fe^{3+} and vacancies on the bulk modulus of bridgmanite that we observed suggests that accurate determination and comparison of the compressibility of bridgmanites may be reliable only if the composition (including $Fe^{3+}/\Sigma Fe$) and the structure of the material are known in detail.

A recent precise study of iron-bearing bridgmanite (*30*) demonstrates that in the case of the charge substitution mechanism, the density and bulk modulus of bridgmanite vary linearly with the Fe content. Using equations reported in the study by Dorfman and Duffy (*34*), at a representative mid-mantle depth of 1850 km (80 GPa), the density and bulk modulus of bridgmanite with composition $Fe_{0.88}SiO_3$ are estimated to be ρ_{80} = 6.171(4) g/cm^3 and $K_{80,300}$ = 556(24) GPa. Using our data, we obtained ρ_{80} = 5.99(1) g/cm^3 and $K_{80,300}$ = 480(15) GPa, and bulk velocity heterogeneity parameter $\partial \ln V_B/\partial X_{Fe}$ = 0.16 [versus ~0.10 in the study by Glazyrin *et al.* (*12*) and Dorfman and Duffy (*34*), a parameter that is almost independent of temperature at Earth's lower mantle pressures (*12*)]. Consequently, for oxidized parts of the lower mantle (for example, subducted slabs) and for relevant chemical compositions, the variation of $Fe^{3+}/\Sigma Fe$ can lead to significant changes in the bulk sound velocity of bridgmanite (exceeding 2%), demonstrating the importance of iron oxidation state for interpreting seismic tomography data (*12*). Moreover, it is now generally accepted that variations in iron content may be one of the major sources of lateral seismic

heterogeneities in Earth's lower mantle (*35*). Our results suggest that incorporation of ferric iron on the A-site of bridgmanite, accompanied by the formation of vacancies, considerably affects the bulk sound velocity and increases the heterogeneity parameter $\partial \ln V_B/\partial X_{Fe}$ by about 60%. Thus, substantially smaller variations in iron content may be required to explain the seismic tomography data (*35*).

MATERIALS AND METHODS

Materials

The material used in this study consisted of single crystals of bridgmanite with different compositions: $Mg_{0.83}Fe_{0.17}Al_{0.06}Si_{0.94}O_3$ (FE17), $Mg_{0.86}Fe_{0.14}Al_{0.04}Si_{0.96}O_3$ (FE14), $Mg_{0.60}Fe_{0.40}Si_{0.63}Al_{0.37}O_3$ (FE40), and skiagite-majorite garnet $(Fe^{2+}_{0.64(2)}Fe^{3+}_{0.24(2)})Si_{1.00(3)}O_3$. The details of samples FE17, FE14, and FE40 were described elsewhere (*12*, *15*, *36*). Mg,Al-free Fe-bridgmanite was synthesized from skiagite-majorite garnet from the same batch that was used in a previous study (*25*).

MA experiments

MA experiments for studying the stability of skiagite were performed at Bayerisches Geoinstitut, Bayreuth, at pressures up to 23 GPa and temperatures up to 1800 K. The starting mixture with the skiagite composition ($Fe_3Fe_2Si_3O_{12}$) was prepared from pure oxides $Fe_{0.94}O$, Fe_2O_3, and SiO_2. The mixtures were loaded into a Re capsule with a 1-mm diameter and 1.8-mm length and heated for 30 min. A $W_{97}Re_3$-$W_{75}Re_{25}$ thermocouple was used to monitor the temperature. According to x-ray powder diffraction, the synthesized sample consists of mixtures of oxides/stishovite, $Fe_{1-x}O$, and Fe_4O_5 (fig. S4).

Microprobe

Chemical compositions of the samples recovered from the MA experiments were characterized using wavelength-dispersive x-ray microprobe analysis (JEOL JXA-8200; focused beam; accelerating voltage of 15 keV and beam current of 15 nA). Metallic Fe and quartz were used as standards for Fe and Si, respectively, with atomic number effects, absorption, and fluorescence correction.

DAC experiments

The crystals of bridgmanite with different compositions in sizes from ~10 × 10 × 5 μm^3 to ~20 × 20 × 7 μm^3 were selected and tested before being loaded into a DAC using an in-house high-brilliance rotating anode diffractometer (*16*).

We used cylindrical-type DACs (*37*) in all experiments. Boehler-Almax–designed diamonds with a culet size of 250 μm were used for measurements less than 70 GPa. Above this pressure, diamonds with 120-μm culet size were used. The sample chamber was prepared by drilling a hole in the center of a 200-μm-thick Re gasket preindented to 20 μm. All DACs were loaded with Ne to achieve quasi-hydrostatic conditions and as a pressure standard. For pressure measurements below 15 GPa, small ruby chips were loaded.

Synchrotron x-ray diffraction

SCXRD experiments were performed at the APS, Argonne National Laboratory, Argonne, United States, at beamline 13 ID-D [GSECARS (GeoSoilEnviroCARS)]; at the ESRF, Grenoble, France, at the ID09A and ID27 beamlines; and at the DESY at PETRA III, Hamburg, Germany, at the extreme conditions beamline P02.2.

High-pressure and high-temperature experiments at 13 ID-D were performed using x-rays with a wavelength of 0.31 Å. The beam was focused with a Kirkpatrick-Baez double-mirror system to dimensions of 10 × 10 μm^2. Diffraction patterns were collected using a MarCCD detector, and the position of the detector was calibrated using a LaB_6 standard. The sample was heated in situ using a Nd:YAG double-sided laser-heating system, and temperatures were measured from both sides by spectroradiometry (*38*).

At the ESRF on beamline ID09A, we used a mar555 flat panel detector and an x-ray wavelength of 0.415 Å with a beam spot size of ~10 × 10 μm^2, whereas on beamline ID27 the parameters were as follows: λ = 0.37 Å; beam size, 3 × 3 μm^2, using PerkinElmer flat panel detector. At the extreme conditions beamline P02.2 at PETRA III, we used an x-ray wavelength of λ = 0.2903 Å and PerkinElmer detector, and the beam size was 3 × 8 μm^2. The positions of the detectors were calibrated using Si or CeO_2 standards.

Single-crystal diffraction data were collected in two modes—by continuous rotation of the cell around the omega axis ("wide scans") from −20° to +20° for in situ high-pressure, high-temperature data acquisition and from −38° to +38° ("step scans") for the temperature-quenched sample (that is, without laser-heating setup) by narrow 0.5° omega scanning. Pressure was determined using the Ne equation of state (*39*). In some experiments, a small (linear dimensions less than 5 μm) piece of gold was loaded at the edge of the pressure chamber to allow an accurate alignment of the cell with respect to the goniometer rotational axis.

The two-dimensional (2D) diffraction images were first analyzed using Dioptas software (*40*). Data processing (peak intensity integration, background evaluation, cell parameters, space group determination, and absorption correction) was performed using CrysAlis^{Pro} 171.36.28 (*41*) software with implemented SCALE3 ABSPACK scaling algorithm. Structures were solved by the direct method using SHELXS (*42*) software implemented in an X-Seed package (*43*). Structure refinement of integrated intensities was performed using SHELXL. Full-profile refinement of powder patterns was conducted using GSAS (General Structure Analysis System) software with a graphical interface, EXPGUI (*44*). Polyhedral volumes were calculated in VESTA (Visualization for Electronic and STructural Analysis) software (*45*).

SUPPLEMENTARY MATERIALS

Supplementary material for this article is available at http://advances.sciencemag.org/cgi/content/full/2/7/e1600427/DC1

fig. S1. Parts of the integrated diffraction images of bridgmanite $Mg_{0.86}Fe_{0.14}Al_{0.04}Si_{0.96}O_3$ (FE14) collected before (lower curve) and during (upper curve) laser heating.

fig. S2. Full high-resolution 2D wide-scan x-ray diffraction images of bridgmanite samples FE14, FE17, and FE40.

fig. S3. Representative polyhedral structural model of orthorhombic bridgmanite.

fig. S4. Backscattered electron image of skiagite starting composition at 23 GPa and 1600°C (run S6151).

fig. S5. Typical powder x-ray diffraction patterns of skiagite-majorite garnet that was laser-heated at different pressures and temperatures (St, stishovite; hFe_3O_4, orthorhombic $CaTi_2O_4$-type Fe_3O_4; Pv, perovskite-structured phase).

fig. S6. Crystal structure of Fe_4O_5 obtained as the product of decomposition of skiagite-majorite garnet in a laser-heated DAC at 39(1) GPa and 2250(100) K (see table S4 for crystallographic data).

fig. S7. Variation with pressure of the normalized unit-cell parameters for three bridgmanites—Fe-bridgmanite (this study), $(Mg_{0.96},Fe_{0.04})SiO_3$ (*32*), and $Mg_{0.60}Fe_{0.40}Si_{0.63}Al_{0.37}O_3$ (*12*).

fig. S8. Effect of Fe^ASiO_3, $Fe^AAl^BO_3$, and $Fe^{3+,A}_{2/3}SiO_3$ substitutions in bridgmanite on the bulk modulus ("A" and "B" denote structural positions; see table S3 for references).

table S1. Crystallographic data for Fe,Al bridgmanite samples FE14, FE17, and FE40 at selected pressures before and after laser heating at different temperatures.

table S2. Crystallographic data for $(Fe^{2+}_{0.64(2)}Fe^{3+}_{0.24(2)})Si_{1.00(3)}O_3$ bridgmanite at selected pressures.
table S3. Compressibility of bridgmanite with different compositions.
table S4. Crystallographic data of Fe_4O_5.

REFERENCES AND NOTES

1. O. Tschauner, C. Ma, J. R. Beckett, C. Prescher, V. B. Prakapenka, G. R. Rossman, Discovery of bridgmanite, the most abundant mineral in Earth, in a shocked meteorite. *Science* **346**, 1100–1102 (2014).
2. M. Murakami, Y. Ohishi, N. Hirao, K. Hirose, A perovskitic lower mantle inferred from high-pressure, high-temperature sound velocity data. *Nature* **485**, 90–94 (2012).
3. L.-G. Liu, Post-oxide phases of olivine and pyroxene and mineralogy of the mantle. *Nature* **258**, 510–512 (1975).
4. S.-H. Shim, T. S. Duffy, G. Shen, Stability and structure of $MgSiO_3$ perovskite to 2300-kilometer depth in Earth's mantle. *Science* **293**, 2437–2440 (2001).
5. D. Andrault, Evaluation of (Mg,Fe) partitioning between silicate perovskite and magnesiowustite up to 120 GPa and 2300 K. *J. Geophys. Res.* **106**, 2079–2087 (2001).
6. M. Murakami, K. Hirose, K. Kawamura, N. Sata, Y. Ohishi, Post-perovskite phase transition in $MgSiO_3$. *Science* **304**, 855–858 (2004).
7. S. K. Saxena, L. S. Dubrovinsky, P. Lazor, Y. Cerenius, P. Häggkvist, M. Hanfland, J. Hu, Stability of perovskite ($MgSiO_3$) in the Earth's mantle. *Science* **274**, 1357–1359 (1996).
8. L. Zhang, Y. Meng, W. Yang, L. Wang, W. L. Mao, Q.-S. Zeng, J. S. Jeong, A. J. Wagner, K. A. Mkhoyan, W. Liu, R. Xu, H.-k. Mao, Disproportionation of $(Mg,Fe)SiO_3$ perovskite in Earth's deep lower mantle. *Science* **344**, 877–882 (2014).
9. D. Andrault, G. Fiquet, Synchrotron radiation and laser heating in a diamond anvil cell. *Rev. Sci. Instrum.* **72**, 1283–1288 (2001).
10. S. M. Dorfman, S. R. Shieh, Y. Meng, V. B. Prakapenka, T. S. Duffy, Synthesis and equation of state of perovskites in the $(Mg,Fe)_3Al_2Si_3O_{12}$ system to 177GPa. *Earth Planet. Sci. Lett.* **357–358**, 194–202 (2012).
11. W. L. Mao, G. Shen, V. B. Prakapenka, Y. Meng, A. J. Campbell, D. L. Heinz, J. Shu, R. J. Hemley, H.-k. Mao, Ferromagnesian postperovskite silicates in the D″ layer of the Earth. *Science* **101**, 15867–15869 (2004).
12. K. Glazyrin, T. Boffa Ballaran, D. J. Frost, C. McCammon, A. Kantor, M. Merlini, M. Hanfland, L. Dubrovinsky, Magnesium silicate perovskite and effect of iron oxidation state on its bulk sound velocity at the conditions of the lower mantle. *Earth Planet. Sci. Lett.* **393**, 182–186 (2014).
13. A. S. Wolf, J. M. Jackson, P. Dera, V. B. Prakapenka, The thermal equation of state of (Mg, Fe)SiO_3 bridgmanite (perovskite) and implications for lower mantle structures. *J. Geophys. Res. Solid Earth* **120**, 7460–7489 (2015).
14. R. E. Cohen, Y. Lin, Prediction of a potential high-pressure structure of $FeSiO_3$. *Phys. Rev. B* **90**, 140102 (2014).
15. I. Kupenko, C. McCammon, R. Sinmyo, C. Prescher, A. I. Chumakov, A. Kantor, R. Rüffer, L. Dubrovinsky, Electronic spin state of Fe, Al-containing $MgSiO_3$ perovskite at lower mantle conditions. *Lithos* **189**, 167–172 (2014).
16. L. Dubrovinsky, N. Dubrovinskaia, I. Kantor, F. Nestola, D. Gatta, High-brilliance X-ray system for high-pressure in-house research: Applications for studies of superhard materials. *High Press. Res.* **26**, 137–143 (2006).
17. E. Bykova, thesis, University of Bayreuth (2015).
18. Y. Fei, Y. Wang, L. W. Finger, Maximum solubility of FeO in (Mg, Fe)SiO_3-perovskite as a function of temperature at 26 GPa: Implication for FeO content in the lower mantle. *J. Geophys. Res.* **101**, 11525–11530 (1996).
19. H.-k. Mao, G. Shen, R. J. Hemley, Multivariable dependence of Fe-Mg partitioning in the lower mantle. *Science* **278**, 2098–2100 (1997).
20. Y. Tange, E. Takahashi, Y. Nishihara, K. Funakoshi, N. Sata, Phase relations in the system MgO–FeO–SiO_2 to 50 GPa and 2000°C: An application of experimental techniques using multianvil apparatus with sintered diamond anvils. *J. Geophys. Res.* **114**, B02214 (2009).
21. S. M. Dorfman, Y. Meng, V. B. Prakapenka, T. S. Duffy, Effects of Fe-enrichment on the equation of state and stability of $(Mg,Fe)SiO_3$ perovskite. *Earth Planet. Sci. Lett.* **361**, 249–257 (2013).
22. L. C. Ming, W. A. Bassett, Decomposition of $FeSiO_3$ into FeO + SiO_2 under very high pressure and high temperature. *Earth Planet. Sci. Lett.* **25**, 68–70 (1975).
23. K. Fujino, D. Nishio-Hamane, K. Suzuki, H. Izumi, Y. Seto, T. Nagai, Stability of the perovskite structure and possibility of the transition to the post-perovskite structure in $CaSiO_3$, $FeSiO_3$, $MnSiO_3$, $CoSiO_3$. *Phys. Earth Planet. Inter.* **177**, 147–151 (2009).
24. I. Kupenko, C. McCammon, R. Sinmyo, V. Cerantola, V. Potapkin, A. I. Chumakov, A. Kantor, R. Rüffer, L. Dubrovinsky, Oxidation state of the lower mantle : In situ observations of the iron electronic configuration in bridgmanite at extreme conditions. *Earth Planet. Sci. Lett.* **423**, 78–86 (2015).
25. L. Ismailova, A. Bobrov, M. Bykov, E. Bykova, V. Cerantola, I. Kupenko, C. McCammon, V. Dyadkin, D. Chernyshov, S. Pascarelli, A. Chumakov, L. Dubrovinskaia, N. Dubrovinsky, High-pressure synthesis of skiagite-majorite garnet and investigation of its crystal structure. *Am. Mineral.* **100**, 2650–2654 (2015).
26. B. Lavina, P. Dera, E. Kim, Y. Meng, R. T. Downs, P. F. Weck, S. R. Sutton, Y. Zhao, Discovery of the recoverable high-pressure iron oxide Fe_4O_5. *Proc. Natl. Acad. Sci. U.S.A.* **108**, 17281–17285 (2011).
27. L. S. Dubrovinsky, N. A. Dubrovinskaia, C. McCammon, G. K. Rozenberg, R. Ahuja, J. M. Osorio-Guillen, V. Dmitriev, H.-P. Weber, T. Le Bihan, B. Johansson, The structure of the metallic high-pressure Fe_3O_4 polymorph: Experimental and theoretical study. *J. Phys. Condens. Matter* **15**, 7697 (2003).
28. E. Bykova, L. Dubrovinsky, N. Dubrovinskaia, M. Bykov, C. McCammon, S. V. Ovsyannikov, H.-P. Liermann, I. Kupenko, A. I. Chumakov, R. Rüffer, M. Hanfland, V. Prakapenka, Structural complexity of simple Fe_2O_3 oxide at high pressures and temperatures. *Nat. Commun.* **7**, 10661 (2016).
29. J. P. Brodholt, Pressure-induced changes in the compression mechanism of aluminous perovskite in the Earth's mantle. *Nature* **407**, 620–622 (2000).
30. S. Xu, S.-H. Shim, D. Morgan, Origin of Fe^{3+} in Fe-containing, Al-free mantle silicate perovskite. *Earth Planet. Sci. Lett.* **409**, 319–328 (2015).
31. J. Liu, B. Mysen, Y. Fei, J. Li, Recoil-free fractions of iron in aluminous bridgmanite from temperature-dependent Mössbauer spectra. *Am. Mineral.* **100**, 1978–1984 (2015).
32. T. Boffa Ballaran, A. Kurnosov, K. Glazyrin, D. J. Frost, M. Merlini, M. Hanfland, R. Caracas, Effect of chemistry on the compressibility of silicate perovskite in the lower mantle. *Earth Planet. Sci. Lett.* **333–334**, 181–190 (2012).
33. A. Saikia, T. Boffa Ballaran, D. J. Frost, The effect of Fe and Al substitution on the compressibility of $MgSiO_3$-perovskite determined through single-crystal X-ray diffraction. *Phys. Earth Planet. Inter.* **173**, 153–161 (2009).
34. S. M. Dorfman, T. S. Duffy, Effect of Fe-enrichment on seismic properties of perovskite and post-perovskite in the deep lower mantle. *Geophys. J. Int.* **197**, 910–919 (2014).
35. J. Trampert, F. Deschamps, J. Resovsky, D. Yuen, Probabilistic tomography maps chemical heterogeneities throughout the lower mantle. *Science* **306**, 853–856 (2004).
36. L. Dubrovinsky, T. Boffa-Ballaran, K. Glazyrin, A. Kurnosov, D. Frost, M. Merlini, M. Hanfland, V. B. Prakapenka, P. Schouwink, T. Pippinger, N. Dubrovinskaia, Single-crystal X-ray diffraction at megabar pressures and temperatures of thousands of degrees. *High Press. Res.* **30**, 620–633 (2010).
37. I. Kantor, V. Prakapenka, A. Kantor, P. Dera, A. Kurnosov, S. Sinogeikin, N. Dubrovinskaia, L. Dubrovinsky, BX90: A new diamond anvil cell design for X-ray diffraction and optical measurements. *Rev. Sci. Instrum.* **83**, 125102 (2012).
38. V. B. Prakapenka, A. Kubo, A. Kuznetsov, A. Laskin, O. Shkurikhin, P. Dera, M. L. Rivers, S. R. Sutton, Advanced flat top laser heating system for high pressure research at GSECARS: Application to the melting behavior of germanium. *High Press. Res.* **28**, 225–235 (2008).
39. Y. Fei, A. Ricolleau, M. Frank, K. Mibe, G. Shen, V. Prakapenka, Toward an internally consistent pressure scale. *Proc. Natl. Acad. Sci. U.S.A.* **104**, 9182–9186 (2007).
40. C. Prescher, V. B. Prakapenka, *DIOPTAS*: A program for reduction of two-dimensional X-ray diffraction data and data exploration. *High Press. Res.* **35**, 223–230 (2015).
41. *CrysAlis^{Pro}* (Rigaku, Tokyo, 2006).
42. G. M. Sheldrick, A short history of *SHELX*. *Acta Crystallogr. Sect. A Found. Crystallogr.* **64**, 112–122 (2008).
43. L. J. Barbour, X-Seed — A software tool for supramolecular crystallography. *J. Supramol. Chem.* **1**, 189–191 (2001).
44. B. H. Toby *EXPGUI*, a graphical user interface for *GSAS*. *J. Appl. Cryst.* **34**, 210–213 (2001).
45. K. Momma, F. Izumi, *VESTA 3* for three-dimensional visualization of crystal, volumetric and morphology data. *J. Appl. Cryst.* **44**, 1272–1276 (2011).
46. T. Katsura, A. Yoneda, D. Yamazaki, T. Yoshino, E. Ito, Adiabatic temperature profile in the mantle. *Phys. Earth Planet. Inter.* **183**, 212–218 (2010).
47. M. Sugahara, A. Yoshiasa, Y. Komatsu, T. Yamanaka, N. Bolfan-Casanova, A. Nakatsuka, S. Sasaki, M. Tanaka, Reinvestigation of the $MgSiO_3$ perovskite structure at high pressure. *Am. Mineral.* **91**, 533–536 (2006).

Acknowledgments: We thank I. Kantor for help with laser heating, and we acknowledge the ESRF for provision of synchrotron radiation facilities. We thank S. Tkachev for the technical support with the gas loading at APS. Portions of this research were carried out at the light source PETRA III at DESY. We acknowledge the use of the DESY photon facility. **Funding:** L.D. and N.D. thank Deutsche Forschungsgemeinschaft (DFG) (project nos. DU945/6-1 and DU945/6-2 of the Heisenberg Program and project no. DU 954-8/1) and the Federal Ministry of Education and Research (BMBF), Germany (project no. 5K13WC3), for financial support. A part of this study was performed at GeoSoilEnviroCARS (Sector 13), APS, Argonne National Laboratory. GeoSoilEnviroCARS is supported by the NSF–Earth Sciences (EAR-1128799) and Department of Energy (DOE)–GeoSciences (DE-FG02-94ER14466). This research used resources of the APS, a U.S. DOE Office of Science User Facility operated for the DOE Office of Science by Argonne National Laboratory, under contract no. DE-AC02-06CH11357. This study was partly supported by the Russian Foundation for Basic Research

(project no. 16-05-00419). **Author contributions:** L.I., L.D., and N.D. conceptualized, planned, designed, and coordinated the research; L.I., R.S., C.M., and A.B. synthesized and characterized the starting materials; E.B., M.B., L.I., V.C., C.M., H.-P.L., I.K., M.H., C.P., V.P., and V.S. conducted synchrotron x-ray diffraction experiments; E.B., L.I., L.D., and T.B.B. performed x-ray diffraction analyses; L.I., E.B., and L.D. prepared figures; and L.D. and L.I. wrote the manuscript. All authors discussed the results and commented on the paper. **Competing interests:** The authors declare that they have no competing interests. **Data and materials availability:** All data needed to evaluate the conclusions in the paper are present in the paper and/or the Supplementary Materials. Additional data related to this paper may be requested from the authors.

Submitted 27 February 2016
Accepted 16 June 2016
Published 15 July 2016
10.1126/sciadv.1600427

Citation: L. Ismailova, E. Bykova, M. Bykov, V. Cerantola, C. McCammon, T. Boffa Ballaran, A. Bobrov, R. Sinmyo, N. Dubrovinskaia, K. Glazyrin, H.-P. Liermann, I. Kupenko, M. Hanfland, C. Prescher, V. Prakapenka, V. Svitlyk, L. Dubrovinsky, Stability of Fe,Al-bearing bridgmanite in the lower mantle and synthesis of pure Fe-bridgmanite. *Sci. Adv.* **2**, e1600427 (2016).

ScienceAdvances
AAAS

Stability of Fe,Al-bearing bridgmanite in the lower mantle and synthesis of pure Fe-bridgmanite

Leyla Ismailova, Elena Bykova, Maxim Bykov, Valerio Cerantola, Catherine McCammon, Tiziana Boffa Ballaran, Andrei Bobrov, Ryosuke Sinmyo, Natalia Dubrovinskaia, Konstantin Glazyrin, Hanns-Peter Liermann, Ilya Kupenko, Michael Hanfland, Clemens Prescher, Vitali Prakapenka, Volodymyr Svitlyk and Leonid Dubrovinsky (July 15, 2016)

Sci Adv 2016, 2:.
doi: 10.1126/sciadv.1600427